Laser and Particle Beams (2016), *34*, 284–293.
© Cambridge University Press, 2016 0263-0346/16
doi:10.1017/S0263034616000112

Numerical modeling of radiative recombination during ionization of atoms by means of particle-in-cell simulation

E. KHALILZADEH,[1,2] J. YAZDANPANAH,[2] J. JAHANPANAH,[1] AND A. CHAKHMACHI[2]

[1]Department of Physics, Kharazmi University, 49 Mofateh Ave, P. O. Box 15614, Tehran, Iran
[2]The Plasma Physics and Fusion Research School, Tehran, Iran

(Received 3 December 2015; Accepted 29 January 2016)

Abstract

In this paper, a heuristic algorithm based on particle-in-cell (PIC) simulation is introduced to investigate the harmonic generation during the ionization and formation of plasma by a non-relativistic laser field when it propagates through hydrogen atoms. The harmonic generation is considered for the radiative recombination of an ionized electron with its nearest ion. The ionization algorithm is improved by considering the Stark effect and nonzero velocity for ionized electrons. Energy conservation is evaluated during the recombination process. In our code, for the first time, Maxwell's equations are integrated for harmonic fields in a separate mesh using the artificial recombination current as a source term. The simulation results are then used to illustrate the intensity spectrum of generated fields. It is shown that the initial momentum of ionized electrons affects the harmonic spectrum because the energy of radiated photons varies with the electron energy.

Keywords: Harmonic generation; Ionization; Monte Carlo; Particle-in-cell simulation; Radiative recombination

1. INTRODUCTION

The ionization process of atoms and the plasma evolution by implementing a high intensity optical field (an ultra-short laser pulse) are of general interest in plasma physics, because of the different applications including inertial confinement fusion, laser-plasma accelerator, and X-ray lasers. It is turned out that the ionization process by a non-relativistic intense laser pulse ($I < 10^{18}$ w/cm^2) can significantly influence the laser–plasma interaction. In this way, pre-pulse effects due to ionization can strongly influence the main pulse propagation (Hosokai *et al.*, 2006). The ionization effects have extensively been investigated theoretically and experimentally to realize the important phenomena such as above threshold ionization (Becker *et al.*, 2002; Frolov *et al.*, 2014), laser frequency blue shifting (Chessa *et al.*, 1999), ionization induced diffraction (Tripathi *et al.*, 2010), self-defocusing (Efimenko & Kim, 2011), and ring formation (Esarey *et al.*, 1997).

The detailed study of ionization processes is rather complicated even by exploiting the recent methods of radiation and particle beam generation (Liu *et al.*, 2011; Wang *et al.*, 2013). The field-ionized plasma differs completely from the commonly known plasma in the sense of electron–ion correlation. In the case of the field-ionized plasma, the electron and ion are strongly correlated. In this case, the electron can frequently reach the parent ion vicinity during the field interaction. It is worth mentioning that except for trapped particles, the electron trajectory is always enclosed in the plasma. When the electron returns to the original ion, interesting radiation phenomena like dipole radiation become possible. In this way, the strong nonlinear effects such as the generation of highly energetic photons (high harmonic generation, HHG) happen. HHG is firstly explained by semi-classical (Corkum, 1993; Schafer *et al.*, 1993) and quantum mechanical (Lewenstein *et al.*, 1994) three-step model, which is designed according to the response of a single atom in relatively weak electromagnetic fields (for example 10^{13}~10^{14} w/cm^2, for a hydrogen atom). Based on this model, the electronic wave function of an atom is partially freed by a strong laser field [the wave function of the electron can be expressed as $\psi(r,t) = \alpha_0\psi_0(r,t) + \alpha_p\psi_p(r,t)$, where $\psi_0(r,t)$ is the ground state and $\psi_p(r,t)$ is a continuum state with the momentum p. α_0 and α_p represent the population of these states]. The ionized electron is accelerated in the local fields and finally the ionized and bound-state portions

Address correspondence and reprint requests to: Elnaz Khalilzadeh, Department of Physics, Kharazmi University, 49 Mofateh Ave, P. O. Box 15614, Tehran, Iran and The Plasma Physics and Fusion Research School, Tehran, Iran. E-mail: el_84111005@aut.ac.ir

https://doi.org/10.1017/S0263034616000112 Published online by Cambridge University Press

of the electronic wave packet interfere with each other giving rise to a strong dipole response that leads to the emission of highly energetic photon along with the recombination of the electron with the bound state. The maximum energy, cut-off energy, that can be generated within this model is $I_p + 3.17\ U_p$, where I_p and U_p are the binding energy of the electron in the atom and the ponderomotive energy in the laser field, respectively. The detailed study of HHG in this regime was one of the most often studied aspects of intense laser physics during the past decades (Mocek *et al.*, 2005; Strelkov, 2006; Ciappina *et al.*, 2007; Ozaki *et al.*, 2007; Colosimo *et al.*, 2008; Shiner *et al.*, 2009; Falcao-Filho *et al.*, 2009; Ghimire *et al.*, 2010; Gkortsas *et al.*, 2011; Klaiber *et al.*, 2012; Bleda *et al.*, 2013).

However, ionization occurs immediately after the laser intensity is increased to a higher level (this happens in many practical cases). In this case, the electron wave function in the majority of its closed trajectory is completely free ($\alpha_0 = 0$) and it can approach to the ground state wave function only through the spontaneous emission process (radiative recombination) (Kohler *et al.*, 2010). It should be noted that the amount of this laser intensity depends on the type of atom (e.g., this intensity for hydrogen atom is $I > 10^{15}\ \mathrm{w/cm^2}$). The purpose of this paper is to investigate the plasma radiation that is produced in this regime. In this way, a heuristic algorithm based on particle-in-cell (PIC) code is introduced for the simulation of radiative recombination during the ionization and formation of plasma when a laser pulse with intensity $10^{16}\sim10^{17}\ \mathrm{w/cm^2}$ is passed through hydrogen atoms.

PIC is one of the most successful numerical methods, which is exploited to study the laser–plasma interactions (Birdsall *et al.*, 1991; Hockney & Eastwood, 1998; Yazdanpanah & Anvary, 2012). The general distribution functions are statistically derived in phase space by solving the Maxwell equations and Lorentz equations of motion, simultaneously. The PIC method employs the fundamental equations with a minimum number of approximations so as to preserve the physical notions. Therefore, unlike the single particle model, the space charge and other collective effects in the field-ionized plasma are taken into account in our PIC model. Therefore, the results of the PIC simulation can be more precise than the numerical calculation using the single particle model. The ionization phenomena have already been studied by considering the field ionization calculation in PIC method in the absence of radiative recombination (Janulewicz *et al.*, 1996; Bruhwiler *et al.*, 2003; Kemp *et al.*, 2004; Chen *et al.*, 2013). In our paper, two Monte Carlo packages are simultaneously added to the usual one-dimensional (1D)-2 V PIC (Yazdanpanah & Anvary, 2012) for considering the ionization and the radiative recombination to measure the harmonics that are generated during the ionization of hydrogen atoms. The ionization process is modified according to the following considerations:

- The theoretical and numerical expressions (Landau & Lifshitz, 1965; Mur & Popov, 1993; Bauer & Mulser, 1999) for the ionization rate are considered according to the value of the electric field strength.
- In the presence of the laser electric field, the Stark shift of the ground state of hydrogen atom is implemented according to Eq. (7) (Mur & Popov, 1993).
- Despite the previous works, nonzero initial momentum is envisaged for the ejected electrons (Delone & Krainov, 1991; Krainov & Shokri, 1995).

The energy gain produced by recombination is considered to satisfy energy conservation by introducing an artificial recombination current, in consistence with the case of ionization. By the use of this artificial current, Maxwell's equations are solved in the separate mesh to calculate the generated fields by harmonic emissions. The simulation results are presented for the responses of the formed plasma and the harmonic generated fields.

It should be noted that the harmonics investigated in this work differ from the harmonic generation in laser–solid interactions due to the nonlinear relativistic oscillation of the plasma components (Shuai *et al.*, 2002; Dromey *et al.*, 2009; Shoucri & Afeyan, 2010; Dollar *et al.*, 2013). This area is completely classical in nature and differs from our case, which is based on quantum mechanics.

The paper is organized as follows: Section 2 contains a general presentation of the physical description of the model. In Section 3, we describe our numerical PIC code and study ionization and recombination processes step by step. We then illustrate the simulation results in Section 4. The summary is given in Section 5.

2. PHYSICAL DESCRIPTION

When an atom is exposed to an ultrahigh optical intensity, electrons can be liberated from the atom through different mechanisms. Keldysh (1964) introduced the parameter γ as

$$\gamma = \frac{\omega_L \sqrt{2I_p}}{E}, \tag{1}$$

and demonstrated that the values $\gamma \ll 1$ and $\gamma \gg 1$ are corresponding to the Tunneling Ionization (TI) and multiphoton ionization, respectively. In Eq. (1), I_p, ω_L, and E are the respective atomic ionization potential, the frequency and amplitude of laser electric field (atomic units will be used throughout this section). In the case $\gamma \ll 1$, when the atom is in an external field, the Coulomb potential barrier is lowered and the electron can tunnel through this barrier. When the laser electric field is strong enough, such that $E > E_{critical}$ [Bauer has shown that this critical value for atomic hydrogen is given by $E_{critical} = 0.146 a.u.$ (Bauer, 1997)], the electron is able to escape (not to tunnel) over the barrier formed by the Coulomb potential and the laser field. This ionization mechanism is called Barrier Suppression Ionization (BSI). The

https://doi.org/10.1017/S0263034616000112 Published online by Cambridge University Press

released electron by field ionization is localized around the nucleus at the distance R_0. R_0 is comparable with the Bohr radius (the size of the Bohr radius is $a_0 = \hbar/m_e c\alpha$ that $\hbar$, m_e, c, and α are reduced Planck's constant, the electron rest mass, the speed of light in vacuum, and the fine structure constant, respectively).

One of the most studied nonlinear phenomena that can occur during the ionization of atoms is HHG, in which the system emits radiation at multiples of the laser frequency. In this paper, we want to introduce a new numerical model based on PIC simulation to investigate the harmonic generation during the ionization. In this way, the following expressions can elaborate the model configuration:

(1) We consider high intensities in $\gamma \ll 1$ (laser pulse with peak intensity $10^{16} \sim 10^{17}$ w/cm^2 and wavelength $\lambda_L = 1$ μm). In this case, the hydrogen atoms are immediately ionized. Based on strong-field approximation (Keldysh, 1964; Faisal, 1973; Reiss, 1980) the electron wave function becomes completely free. Therefore, the wave function in the continuum state can be described by a plan wave ($|p\rangle$).

(2) The electron in the continuum state treats as a free particle moving in the local electric field with no effect of atomic potential. Furthermore, the intensities are large enough ($10^{16} \sim 10^{17}$ w/cm^2) to ignore the continuum–continuum transitions (Lewenstein *et al.*, 1994) (The continuum–continuum transitions occur when the velocity of the ionized electron is low. Here, due to the high laser intensity, these transitions can be ignored).

(3) The electron in continuum state could transit to the ground state of hydrogen atom ($|0\rangle$) and produce harmonic generation through radiative recombination. The transition amplitude is given by the following equation in the length gauge (Lewenstein *et al.*, 1994),

$$\mu = |\langle p|r|0\rangle|^2 = \left(\frac{2^7 \alpha_I{}^{5/2}}{\pi^2}\right) \frac{p^2}{(p^2+\alpha_I)^6} \tag{2}$$

where $\alpha_I = 2I_p = 1$. We consider the recombination of an electron with its nearest Hydrogen ion. According to the quasi-classical three-step model, the electrons are only able to return to the parent ions, depending on the phase of the electric field at the instant of ionization. In this model, most electrons are produced at unfavorable phases of the electric field and never return to the core. Although this process properly explains various features of HHG, it does not mean that the other atoms play no role. However, an electron freed through ionization may recombine either with its parent ion or with other ions in its vicinity. For example, consider $x = R$ to be the distance between a parent ion with respect to that of recombined with an electron in a linear-polarized electric field ($E = E_0 \cos(\omega_L t)$). By solving the equation of motion in the non-relativistic intensity for the electron position under the initial conditions $x(t_i) = 0$ and $\dot{x}(t_i) = 0$, we obtain the following relation:

$$R = \frac{E}{\omega_L{}^2}[(\cos(\omega_L t_r) - \cos(\omega_L t_i) + \omega_L(t_r - t_i)\sin(\omega_L t_i)], \tag{3}$$

in which t_i is the ionization time, and t_r the time of the recombination of the electron emitted during the ionization with the nearest neighbor ion. In dependence on the distance R, these times are rather different.

3. ONE DIMENSION PIC SIMULATION

In this paper, the simulation box is extended by 170 μm in x direction (1D geometry). A uniform neutral Hydrogen gas that is initially distributed within the region of 60–120 μm, was used as the plasma source. A laser pulse of Gaussian profile enters with a linear polarization in the y direction from the left side of simulation box and passes through the hydrogen atoms, as illustrated in Figure 2. The laser pulse wavelength is $\lambda_L = \lambda_0 = 1$ μm and the number density of the initial neutral hydrogen atoms is 0.007 n_{cr}, where $n_{cr} = \pi m_e c^2/e^2 \lambda_L{}^2$ represents the critical density. In this simulation, we use 20 macro-particles/cell that are initially distributed within the region of 60–120 λ_L, uniformly. The grid spacing is $\delta x = 0.005$ μm throughout simulations. As mentioned in the previous section, the electron radiation is considered as a three-step process: Ionization, acceleration in a local field, and radiative recombination with the nearest center. Our PIC algorithm process is developed according to these three steps. In this way, two Monte Carlo packages are added to the usual relativistic and fully electromagnetic 1D-2 V PIC code algorithm (Yazdanpanah & Anvary, 2012) to consider the ionization and the recombination steps. In the following, we explain the three steps in detail.

3.1. Fundamental Equations of Usual Electromagnetic 1D-2 V PIC Code

In the PIC method, the gas is represented by a number of macro-particles that move in a domain described by a computational mesh. All the volume of particles is divided by a set of mesh cells and every point of the considered space belongs to one of the existing cells of a mesh. The fixed and time independent set of cells is usually used for this task. A number of finite particles present the continuous medium of plasma or beam. Each finite particle has a mass, charge state, and coordinates in the phase space of motion. In order to describe atomic processes and to effectively calculate Coulomb interactions among the charged particles, the best way is to have densities of each type of physical particle in the mesh. A sufficient number of finite particles of each species should be in each cell for this purpose. The number of real particles

https://doi.org/10.1017/S0263034616000112 Published online by Cambridge University Press

corresponding to a super-particle must be chosen such that sufficient statistics can be collected on the particle motion.

The usual PIC algorithm is fully described by one of the authors (Yazdanpanah & Anvary, 2012). In the following, we only explain the basic equations in the PIC simulation. For many types of problems, the PIC method is relatively intuitive and straightforward to implement. A diagrammatic representation of one time step of the simulation is illustrated in Figure 1. As shown in this figure, the method typically includes the following procedures:

- Integration of the (Newton–Lorentz) motion equations:

$$\frac{d\vec{v}}{dt} = \frac{q}{m}(\vec{E} + \frac{\vec{v}}{c} \times \vec{B}) \tag{4}$$

  In Eq. (4), $\vec{v}$, $\vec{E}$ and $\vec{B}$ are the charged particle velocity, the electric and magnetic field in plasma and m and q are the particle mass and charge, respectively.
- Interpolation of charge and current source terms to the field mesh.
- Computation of the fields on mesh points using the following Maxwell equations:

$$\begin{aligned} \frac{\partial \vec{E}}{\partial t} &= 4\pi\vec{j} - c\vec{\nabla} \times \vec{B} \\ \frac{\partial \vec{B}}{\partial t} &= c\vec{\nabla} \times \vec{E} \end{aligned} \tag{5}$$

  $\vec{j}$ is the current.
- Interpolation of the fields from the mesh to the particle locations.

In our code, reflecting and open boundary conditions have been applied to the particles and fields, respectively. The results of this code can be accurate, as long as the formed plasma is non-collisional. The 1D geometry is applicable here for the laser spot size larger than the laser wavelength and for the Rayleigh length larger than the laser propagation length.

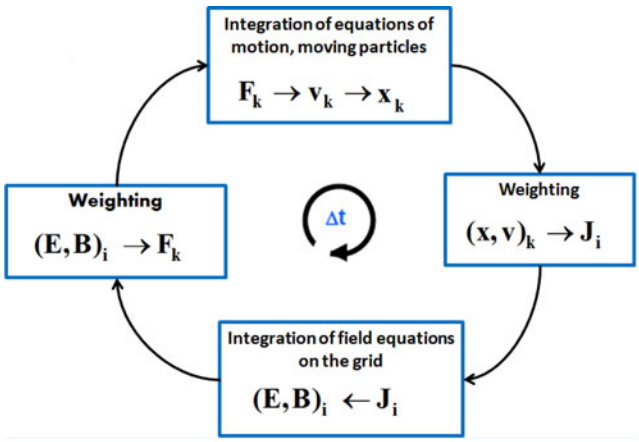

Fig. 1. A diagrammatic representation of one time step of the PIC simulation. The particles are numbered $k = 1, 2, 3,\ldots$; the grid indices are i.

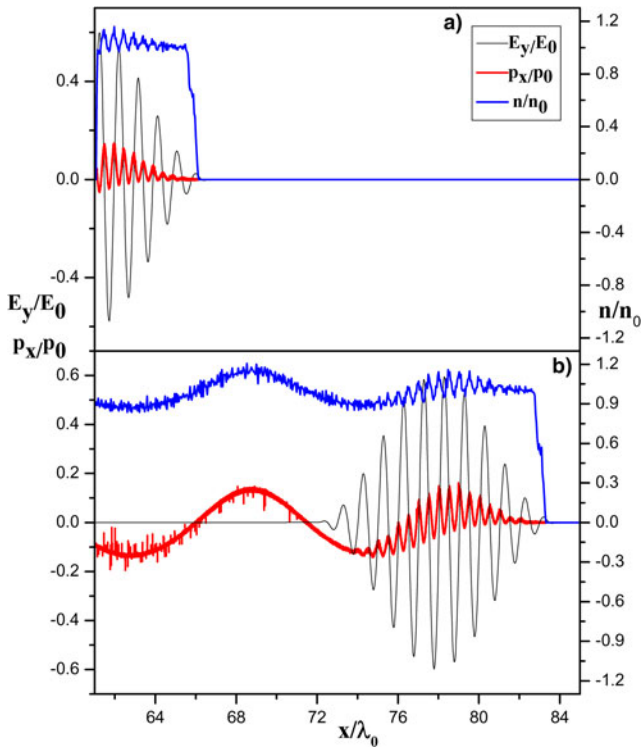

Fig. 2. The PIC simulation results for the laser electric field E_y (black curve) normalized by $E_0 = \omega_L m_e c/q_e$, the density of the ionized electrons n_e (blue curve) normalized by the initial H atoms density n_0, and the momentum of the electrons p_x (red curve) normalized by $p_0 = m_e c$ for $a_0 = 0.6$ at (a) $t_1 = 40\omega_L{}^{-1}$, and (b) $t_2 = 160\omega_L{}^{-1}$.

3.2. Field Ionization

There are many theoretical reports about the rate of field ionization for hydrogen atoms in the region of TI and BSI. Bauer and Mulser (1999) have compared their results with a numerical solution of the time-dependent Schrodinger equation for an electron involved in the Coulomb potential of a hydrogen atom. They proposed a combined formula (a combination of theoretical and empirical formula) for the ionization rate, which is used in this paper for the region $E < 0.175$ as

$$w = \begin{cases} \dfrac{4}{E}\exp\left(-\dfrac{2}{3E}\right) & \text{for } E < 0.084 \quad \text{(Landau formula)} \\ 2.4E^2 & \text{for } 0.084 \le E < 0.175 \quad \text{(emprical formula)} \end{cases} \tag{6}$$

The numerical calculations of Mur and Popov in a strong electric field demonstrate that the values of the Stark shift associated with the ground state of hydrogen atom are greatly diminished by increasing the field strength, which is in contrast with the second-order perturbation theory (Mur &

https://doi.org/10.1017/S0263034616000112 Published online by Cambridge University Press

Popov, 1993). In this case, the determined ionization rates can be correctly fitted by the following equation

$$w = 1.29\,E - 0.15 \quad \text{for } 0.175 \le E \le 0.8. \tag{7}$$

It should be noted that the boundary values of electric field in Eqs. (6) and (7) are determined by assuming the continuity of ionization rate. When the number of the ionized electrons increases, the space charge effects are also important; consequently they can be taken into consideration. Therefore, the electric field E in the Eqs. (6) and (7) is considered as the superposition of the laser electric and space charge fields [the atomic units are used in Eqs. (6) and (7)]. Likewise, the electric fields due to the space charge effects are entered into the code by using Maxwell Eq. (5).

Contrary to the most simulation codes, we consider here an initial velocity for the particles just after ionization to achieve the most accurate results. The expression for the rate of ionization in the non-relativistic regime for a fixed value of electron momentum p by linearly polarized radiation was obtained in (Delone & Krainov, 1991; Krainov & Shokri, 1995) as:

$$w(p_{\parallel},\, p_{\perp}) = w(0)\exp\left[-\frac{\omega^2 {p_{\parallel}}^2}{3E^3} - \frac{{p_{\perp}}^2}{E}\right], \tag{8}$$

in which $p_{\parallel}$ and $p_{\perp}$ are the respective components of photoelectron momentum along and normal to the axis of laser field polarization. In Eq. (8), the factor $\exp\left[-\omega^2 {p_{\parallel}}^2/3E^3 - {p_{\perp}}^2/E\right]$ determines the kinetic energy distribution of the ejected electrons. The value of the pre-exponential factor in Eq. (8), $w(0)$, is the same ionization rate as obtained in Eqs. (6) and (7).

The implementation of the ionization process in a PIC code is straightforward. Initially, all electrons are bounded to the atoms. At each time step δt, for each neutral particle, the local electric field and particle ionization parameters [such as ionization potential and the initial momentum that is predicted in the exponential factor of Eq. (8)] are continuously used to calculate the ionization rate $w(t)$. The ionization probability is then given by $p_{\mathrm{i}} = 1-\exp[-w\ (t)\delta t]$, which is usually approximated as $p_{\mathrm{i}} = w(t)\delta t$ in the case of $p_{\mathrm{i}} \ll 1$. The code generates a random number P_0 with a uniform distribution between 0 and 1. If $P_0 < P_{\mathrm{i}}$, the ionization is done and an electron is formed at the location of ion with nonzero velocity. Otherwise, the particle will not be ionized and will be evaluated during the next time step.

According to the energy conservation, the energy loss due to ionization should continuously be considered. This is done by adding an artificial ionization current j_{ion} to the main current in Eq. (5) at each time step. This artificial ionization current $\vec{j}_{\mathrm{ion}}$ is directed along the local electric field $\vec{E}$, and is defined by the following equation (Mulser *et al.*, 1998; Kemp *et al.*, 2004; Chen *et al.*, 2013)

$$\vec{j}_{\mathrm{ion}} = \frac{\vec{E}\, n_{\mathrm{i}}(I_{\mathrm{p}} + U_{\mathrm{k}})}{\delta t \left|\vec{E}\right|^2}, \tag{9}$$

in which n_{i} and U_{k} are associated with the number density of the ionized electrons in each time step (which is calculated in the code, routinely) and their initial energies after ionization, respectively.

3.3. Recombination

In our code, the recombination process is carried out by the following steps: The rate of radiative emission in the dipole approximation is given by (Svelto, 1998):

$$\Gamma_{\mathrm{rad}} = \frac{\omega^3 \mu^2}{3\pi\varepsilon_0 \hbar\, c^3} = \frac{4\alpha\omega^3\mu^2}{3c^3}, \tag{10}$$

where $\omega = [(1/2)mv^2 + I_{\mathrm{p}}]/\hbar$ is the emission frequency, ϵ_0 is the vacuum permittivity, $\hbar$ is the Planck constant, c is the speed of light, and α is the fine structure constant. In Eq. (10), μ is the transition amplitude that is defined in Eq. (2).

At each time step, the charged particles are sorted by their positions. For each ion, the electrons that are located in distance $r \le R_0$ are listed. With the use of Eq. (10), the radiative emission rate is obtained. Then, by adopting the same procedure in the ionization stage, the recombination probability P_{r} is calculated for the first electron according to the list. The code generates a random number P_0 with a uniform distribution between 0 and 1. If $P_0 < P_{\mathrm{r}}$, the recombination is done and a neutral particle is formed at the location of ion with the ion velocity. Otherwise, the recombination probability is calculated for the second electron listed and a new random number is generated. This process will continue, until all electrons that exist in the distance $r \le R_0$ are dealt with.

The energy conservation law also requires that the energy produced by the recombination of electron with ion is added to the electromagnetic field in each cell. This is done by adding an artificial recombination current j_{rec} to the current in Eq. (5) at each time step throughout the simulation. The same as the ionization stage, it is done by introducing an artificial current j_{rec} as

$$\vec{j}_{\mathrm{rec}} = -\frac{\vec{E}_{\mathrm{col}}(r) n_{\mathrm{rec}}(I_{\mathrm{p}} + U_{\mathrm{rec}})}{\delta t \left|\vec{E}_{\mathrm{col}}(r)\right|^2}, \tag{11}$$

where n_{rec} and U_{rec} represent the number density of recombined electrons in each time step (which is calculated by using a counter in the code, routinely) and their kinetic energies, respectively, and $\vec{E}_{\mathrm{col}}(r)$ represents the mean Coulomb field that is exerted on the electron by the ion.

In order to calculate the generated fields by harmonic emissions, in our code for the first time, Maxwell's equations

https://doi.org/10.1017/S0263034616000112 Published online by Cambridge University Press

are solved in the separate mesh utilizing the artificial current j_{rec}. In fact, choosing the separate mesh is necessary in order to avoid mixing the harmonic fields with numerical noise levels. Meanwhile, the initial values of both the harmonic electric and magnetic fields are assumed zero.

4. SIMULATION RESULTS AND DISCUSSION

The plasma response and harmonic spectrum have been calculated by our PIC code for several cases. Figure 2 illustrates the density and momentum of the liberated electrons along the propagation direction x for the normalized laser intensity $a_0 = eE_L/m_e\omega_L c = 0.6$ at (a) $t_1 = 40\,\omega_L{}^{-1}$ and (b) $t_2 = 160\,\omega_L{}^{-1}$. It is evident that the pulse has enough intensity to ionize the hydrogen atoms, instantly. It is seen that a wake wave is expectably excited by the laser pulse in the field-ionized plasma.

The laser electric field E_y/E_0 and harmonic emissions field E_{yh}/E_0 are, respectively, demonstrated by the left and right vertical axes against the horizontal axis x/λ_0 in Figure 3, for $a_0 = 0.6$ at the typical times (a) $t_1 = 40\,\omega_L{}^{-1}$, (b) $t_2 = 120\,\omega_L{}^{-1}$, and (c) $t_3 = 160\,\omega_L{}^{-1}$. The value of harmonic generated field in comparison with the laser pulse field is obvious in each position of this figure. Evidently, the generated field by harmonic emission has a higher amplitude in front of the laser pulse than the other regions of it. This could be due to weak laser fields in this region. Furthermore, it seems that the space charge effect, which achieves the separation of electrons and ions from each other, can prevent the recombination of electrons with ions behind the laser pulse. Because harmonic generation is ceased at high intensities, $I > 10^{15}$ w/cm^2, the energy conversion efficiency is highly affected by the pulse shape, that is, the conversion efficiency is higher at lower intensity regions of the laser pulse. In this way, as far as we are concerned, the total energy conversion efficiency cannot indicate the effectiveness of the process. Here, we give another measure of efficiency (local efficiency) based on the ratio of maximum harmonic field

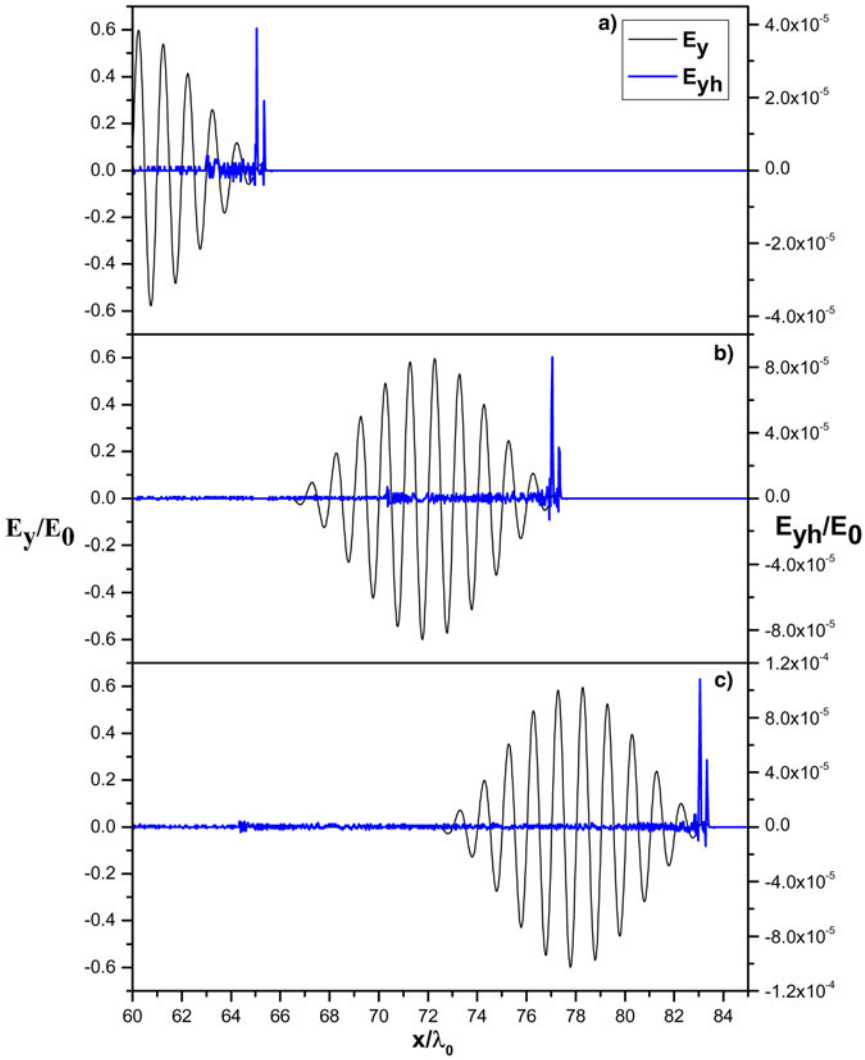

Fig. 3. The PIC simulation results for the laser electric field E_y/E_0 (black curve) and the harmonic electric field E_{yh}/E_0 (blue curve) for $a_0 = 0.6$ at (a) $t_1 = 40\,\omega_L{}^{-1}$, (b) $t_2 = 120\,\omega_L{}^{-1}$, and (c) $t_3 = 160\,\omega_L{}^{-1}$.

https://doi.org/10.1017/S0263034616000112 Published online by Cambridge University Press

amplitude square, $E_{\max-h}$, to the corresponding local main field amplitude square, E_{LM}, as:

$$\eta = \frac{E^2_{h-max}}{E^2_{LM}} \approx 4 \times 10^{-6}. \quad (12)$$

Figure 4 shows the intensity spectrum of the generated fields in Figure 3. The spectrum consists of three parts: The first few harmonics, the plateau for intermediate orders, and the cutoff at the highest orders. Therefore, the general behavior of the present harmonic spectrum is similar to the previous theoretical and experimental works (Lewenstein *et al.*, 1994; Dionissopoulou *et al.*, 1996; Seres *et al.*, 2005; Murakami *et al.*, 2013) in lower intensity, $I \approx 10^{14}$ w/cm^2. Based on the numerical calculation of the single atom model, it has been shown (Corkum, 1993; Schafer *et al.*, 1993) that the maximum photon energy, cut-off energy, that can be generated within this model is $I_p + 3.17\,U_p$. Here, in order to have an order of cut-off energy for the generated harmonic, we calculate cut-off energy for the first cycle of the laser pulse (according to Fig. 3, it is evident that the most harmonic fields are formed in this area). As has been shown in Figure 4, the cut-off of this spectrum happens at a lower value $I_p + 1.32\,U_p$. This difference can be explained by this reason that unlike the single atom model, the space charge (that causes all electron trajectories to be closed) and other collective effects in the field-ionized plasma can affect the harmonics generation process and shift of cutoff energy. It is worth mentioning that the low-order harmonics can be generated with oscillations of electrons density during the nonlinear process of field ionization (Andreev *et al.*, 2003). Because in the PIC simulation the whole feature of nonlinear effects is preserved, these types of harmonics are produced and added to the electric fields. Since the size of these fields is very small compared with the laser fields, they are not distinguishable. However, as mentioned in the previous section, the fields of the generated harmonics are calculated in a separate mesh by means of the artificial current j_{rec} [Eq. (11)], which automatically separates the harmonic fields originated from the radiative recombination with the other fields (including harmonics caused by density oscillation) in plasma.

Figure 5 shows the intensity spectrum of harmonics generated by the amplitudes (a) $a_0 = 0.5$, (b) $a_0 = 0.6$, and (c) $a_0 = 0.7$ at $t = 120\,\omega_L{}^{-1}$. It is evident that the intensity of harmonics is reduced by increasing the intensity of the pulse. This is due to the fact that the electron gains more energy in a strong laser field so that its trapping probability by the potential well of H ion is considerably reduced.

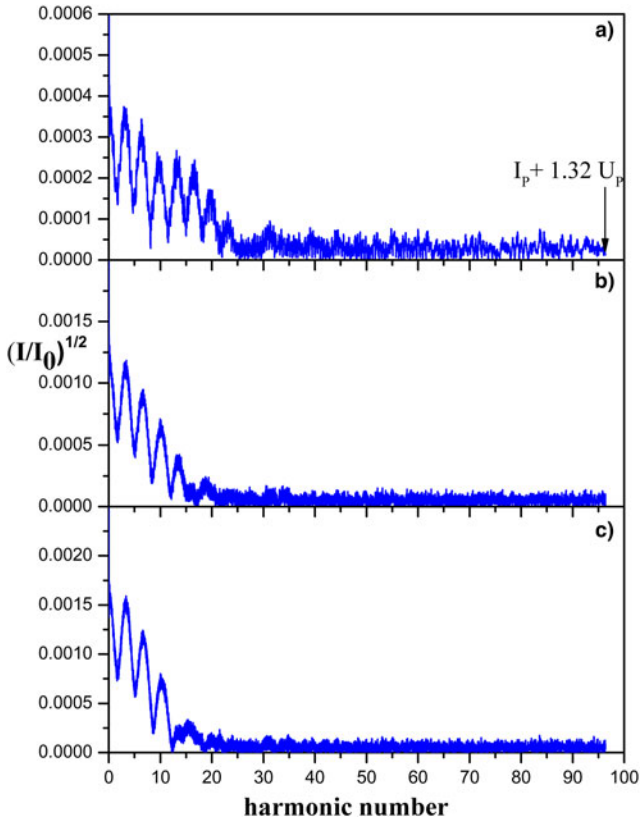

Fig. 4. The PIC simulation results of intensity spectrum for generated field presented in Figure 3 (with the same simulation parameters). The vertical and horizontal axes are corresponding to the square of normalized intensity and harmonic number (k/k_L) respectively.

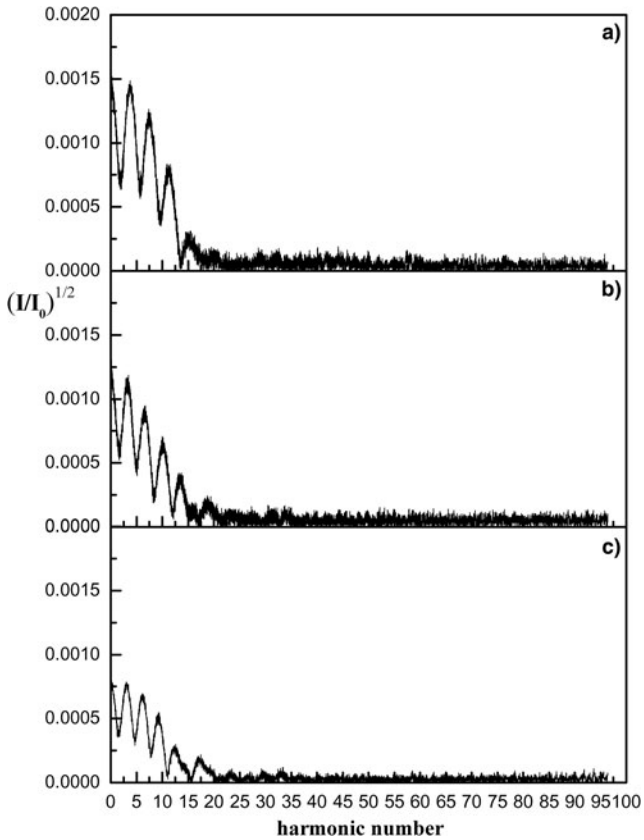

Fig. 5. The PIC simulation results for the harmonic intensity spectrum for (a) $a_0 = 0.5$, (b) $a_0 = 0.6$ and (c) $a_0 = 0.7$.

https://doi.org/10.1017/S0263034616000112 Published online by Cambridge University Press

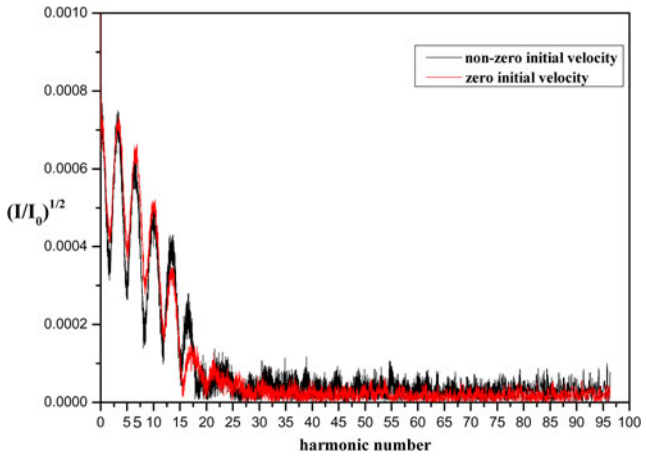

Fig. 6. The PIC simulation results for the harmonic intensity spectrum for $a_0 = 0.6$, (a) nonzero initial velocity of the ionized electrons (black curve), and (b) zero initial velocity of the ionized electrons (red curve).

The initial velocity effect of the ionized electrons on the intensity spectrum is shown in Figure 6, for a pulse with the amplitude $a_0 = 0.6$ at $t = 80\,\omega_L{}^{-1}$. In this figure, the red and black curves show the harmonic spectra for zero and nonzero initial velocity of electrons, respectively. It is clear that the harmonic spectrum is modified by changing the initial momentum of the ionized electrons, because the energy of the radiated photons depends on the electron energy. By comparing the red and black curves, it is realized that the general behavior of harmonic spectrum is not changed by choosing the nonzero initial momentum, but certain changes occur in the intensity of harmonics.

Figure 7 shows the temporal evolution of the electromagnetic and mechanical energies. Time is given in units of laser cycles. Eventually, we come to the conclusion that the sum of electromagnetic and mechanical energies (total energy) is always constant, which confirms the accuracy and validity of our code.

Additionally, the simulation result indicates that the present code can be used for the strict scrutiny of the plasma subjects, in which ionization plays an important role (Janulewicz *et al.*, 1996; Ditmire, 1996; Bauer, 2003; He & Chang, 2005; Eslami & Basereh, 2013; Misra *et al.*, 2014).

5. SUMMARY

In this paper, a novel algorithm based on the PIC simulation is introduced to investigate the radiative recombination during the ionization and formation of plasma when a nonrelativistic laser pulse is passed through the hydrogen atoms. The theoretical and numerical expressions have been exploited for the ionization rate in consistence with the values of the electric field strength. In addition, according to Eq. (7) the Stark shift is considered for the ground state of atoms in the presence of the laser electric field. Despite the pervious codes (Janulewicz *et al.*, 1996; Bruhwiler *et al.*, 2003; Kemp *et al.*, 2004; Chen *et al.*, 2013), the nonzero initial momentum is assigned for the ionized electrons. In our code, two Monte Carlo packages have been added to the usual PIC scheme after the computation of the charge and current and before the integration of Maxwell equations to study the harmonic generation produced by the recombination of the ionized electron. The energy gain of electron recombination has been implemented by introducing an artificial recombination current to save the energy conservation law. This recombination current is vital to calculate the fields of generated harmonics in the separate meshes. In this way, the intensity spectrum of the generated harmonic fields is illustrated. The spectrum is similar to those produced

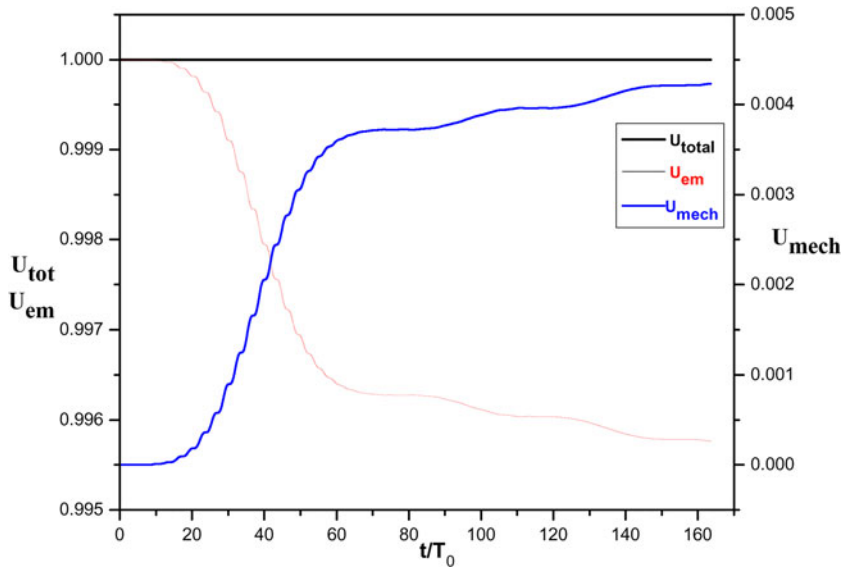

Fig. 7. The PIC simulation results for the temporal evolution of the electromagnetic (red curve), mechanical (blue curve), and total (black curve) energy.

https://doi.org/10.1017/S0263034616000112 Published online by Cambridge University Press

in lower intensities, albeit with some evident differences are also observed. In addition, the initial momenta of the ionized electrons are likely to affect the harmonic spectrum because the energy of the radiated photons varies with the electron energy.

REFERENCES

Andreev, N.E., Veisman, M.E. & Chegotov, M.V. (2003). Third-harmonic generation in an ionized gas and its relation to the residual energy of electrons. *J. Exp. Theor. Phys*. **97**, 554–565.

Bauer, D. (1997). Ejection energy of photoelectrons in strong-field ionization. *Phys. Rev. A* **55**, 2180–2185.

Bauer, D. (2003). Plasma formation through field ionization in intense laser–matter interaction. *Laser Part. Beams* **21**, 489–495.

Bauer, D. & Mulser, P. (1999). Exact field ionization rates in the barrier-suppression regime from numerical time-dependent Schrodinger-equation calculations. *Phys. Rev. A* **59**, 569–577.

Becker, W., Grason, F., Kopold, R., Milosevic, D.B., Paulus, G.G. & Walther, H. (2002). Above-threshold ionization: From classical features to quantum effects. *Adv. At. Mol. Opt. Phys*. **48**, 35–97.

Birdsall, C.K., Langdon, A.B., Vehedi, V. & Verboncoeur, J.P. (1991). *Plasma Physics via Computer Simulations*. Bristol: Adam Hilger.

Bleda, E.A., Yavuz, I., Altun, Z. & Topcu, T. (2013). High-order-harmonic generation from Rydberg states at fixed Keldysh parameter. *Phys. Rev. A* **88**, 043417.

Bruhwiler, D.L., Dimitrov, D.A., Cary, J.R., Esarey, E., Leemans, W. & Giacone, R.E. (2003). Particle-in-cell simulations of tunneling ionization effects in plasma based accelerators. *Phys. Plasmas* **10**, 2022–2030.

Chen, M., Cormier-Michel, E., Geddes, C.G.R., Bruhwiler, D.L., Yu, L.L., Esarey, E., Schroeder, C.B. & Leemans, W.P. (2013). Numerical modeling of laser tunneling ionization in explicit particle-in-cell codes. *J. Com. Phys*. **236**, 220–228.

Chessa, P., De Wispelaere, E., Dorchies, F., Malka, V., Marques, J. R., Hamoniaux, G., Mora, P. & Amiranoff1, F. (1999). Temporal and angular resolution of the ionization-induced refraction of a short laser pulse in helium gas. *Phys. Rev. Lett*. **82**. 552–555.

Ciappina, M.F., Chirilă, C.C. & Lein, M. (2007). Influence of Coulomb continuum wave functions in the description of high order harmonic generation with H_2. *Phys. Rev. A* **75**, 043405.

Colosimo, P., Doumy, G., Blaga, C.I., Wheeler, J., Hauri, C., Catoire, F., Tate, J., Chirla, R., Maech, A.M., Paulus, G.G., Muller, H.G., Agostin, P. & Dimauro, L.F. (2008). Scaling strong-field interactions towards the classical limit. *Nat. phy*. **4**, 386–389.

Corkum, P.B. (1993). Plasma perspective on strong-field multiphoton ionization. *Phys. Rev. Lett*. **71**, 1993–1997.

Delone, N.B. & Krainov, V.P. (1991). Energy and angular electron spectra for the tunnel ionization of atoms by strong low-frequency radiation. *J. Opt. Soc. Am. B* **8**, 1207–1211.

Dionissopoulou, S., Mercouris, T. & Nicolaides, C.A. (1996). Ionization rates and harmonic generation for H interacting with laser pulses of $\lambda = 1064$ nm and peak intensities in the range 2×10^{13}–2×10^{14} W cm^{-2}. *J. Phys. B: At. Mol. Opt. Phys*. **29**, 4787–4794.

Ditmire, T. (1996). Simulations of heating and electron energy distributions in optical field ionized plasmas. *Phys. Rev. E* **54**, 6735–6740.

Dollar, F., Cummings, P., Chvykov, V., Willingale, L., Vargas, M., Yanovsky, V., Zulick, C., Maksimchuk, A., Thomas, A.G.R. & Krushelnick, K. (2013). Scaling high-order harmonic generation from laser-solid interactions to ultrahigh intensity. *Phys. Rev. Lett*. **110**, 175002.

Dromey, B., Bellei, C., Carroll, D.C., Clarke, R.J., Green, J.S., Kar, S., Kneip, S., Markey, K., Nagel, S.R., Willingale, L., Mckenna, P., Neely, D., Najmudin, Z., Krushelnick, K., Norreys, P.A. & Zepf, M. (2009). Third harmonic order imaging as a focal spot diagnostic for high intensity laser-solid interactions. *Laser Part. Beams* **27**, 243–248.

Efimenko, E.S. & Kim, A.V. (2011). Strongly coupled regime of ionization-induced scattering in ultrashort laser-matter interactions. *Phys. Rev. E* **84**, 036408.

Esarey, E., Sprangle, P., Krall, J. & Ting, A. (1997). Self-focusing and guiding of short laser pulses in ionizing gases and plasmas. *IEEE J. Quant. Electron*. **33**, 1879–1914.

Eslami, E. & Basereh, K. (2013). Effects of plasma and ultrashort laser pulse on residual electron energy in optical-field-ionized oxygen plasma. *Laser Part. Beams* **31**, 187–193.

Faisal, F.H.M. (1973). Multiple absorption of laser photons by atoms. *J. Phys. B* **6**, L89–L92.

Falcao-Filho, E.L., Gkortsas, V.M., Gordon, A. & Kartner, F.X. (2009). Analytic scaling analysis of high harmonic generation conversion efficiency. *Opt. Express* **17**, 11217.

Frolov, M.V., Knyazeva, D.V., Manakov, N.L., Geng, J.W., Peng, L.Y. & Starace, A.F. (2014). Analytic model for the description of above-threshold ionization by an intense short laser pulse. *Phy. Rev. A* **89**, 063419.

Ghimire, S., Dichiara, A.D., Sistrunk, E., Agostini, P., Dimauro, L.F. & Reis, D.A. (2010). Observation of high-order harmonic generation in a bulk crystal. *Nat. Phy*. **1847**, 138–141.

Gkortsas, V.M., Bhardwaj, S., L Falcão-Filho, E., Hong, K.H., Gordon, A. & X Kärtner, F. (2011). Scaling of high harmonic generation conversion efficiency. *J. Phys. B: At. Mol. Opt. Phys*. **44**, 045601.

He, B. & Chang, T.Q. (2005). Residual energy in optical-field-ionized plasmas with the longitudinal motion of electrons included. *Phys. Rev. E* **71**, 066411.

Hockney, R. & Eastwood, J. (1998). *Computer Simulation using Particles*. New York: Taylor & Francis Group.

Hosokai, T., Kinoshita, K., Ohkubo, T., Maekawa, A., Uesaka, M., Zhidkov, A., Yamazaki, A., Tomassini, P., Giulietti, A. & Giulietti, D. (2006). Observation of strong correlation between quasimonoenergetic electron beam generation by laser wakefield and laser guiding inside a preplasma cavity. *Phy. Rev. E* **73**, 036407.

Janulewicz, K.A., Grout, M.J. & Pert, G.J. (1996). Electron residual energy of optical-field-ionized plasmas driven by subpicosecond laser pulses. *J. Phys. B: At. Mol. Opt. Phys*. **29**, 901–914.

Keldysh, L.V. (1964). Ionization in the field of a strong electromagnetic wave. *Eksp. Teor. Fiz*. **47**, 1945–1964.

Kemp, A.J., Pfund, R.E.W. & Meyer-ter-Vehn, J. (2004). Modeling ultrafast laser-driven ionization dynamics with Monte Carlo collisional particle in-cell simulations. *Phys. Plasmas* **11**, 5648–5657.

https://doi.org/10.1017/S0263034616000112 Published online by Cambridge University Press

Klaiber, M., Kohler, M.C., Hatsagortsyan, K.Z. & Keitel, C.H. (2012). Optimization of the recollision step in high-order harmonic generation. *Phys. Rev. A* **85**, 063829.

Kohler, M.C., Ott, C., Raith, P., Heck, R., Schlegel, I., Keitel, C.H. & Pfeifer, T. (2010). High harmonic generation via continuum wave-packet interference. *Phy. Rev. Lett*. **105**, 203902.

Krainov, V.P. & Shokri, B. (1995). Energy and angular distributions of electrons resulting from barrier-suppression ionization of atoms by strong low-frequency radiation. *JETP* **80**, 657–661.

Landau, L. & Lifshitz, E. (1965). *Quantum Mechanics*. New York: Butterworth Heinemann.

Lewenstein, M., Balcou, Ph., Ivanov, Yu.M., L'Huillier, A. & Corkum, P.B. (1994). Theory of high-harmonic generation by low-frequency laser fields. *Phys. Rev. A* **49**, 2117–2132.

Liu, J.S., Xia, C.Q., Wang, W.T., Lu, H.Y., Wang, C., Deng, A.H., Li, W.T., Zhang, H., Liang, X.Y., Leng, Y.X., Lu, X.M., Wang, C., Wang, J.Z., Nakajima, K., Li, R.X. & Xu, Z.Z. (2011). All-optical cascaded laser wakefield accelerator using ionization-induced injection. *Phys. Rev. Lett*. **107**, 035001.

Misra, S., Mishra, S.K., Sodha, M.S. & Tripathi, V.K. (2014). Effect of electron-ion recombination on self-focusing/ defocusing of a laser pulse in tunnel ionized plasmas. *Laser Part. Beams* **32**, 21–31.

Mocek, T., Sebban, S., Bettaibi, I., Zeitoun, Ph., Faivre, G., Cros, B., Maynard, G., Butler, A., Mckenna, C.M., Spence, D.J., Gonsavles, A.J., Hooker, S.M., Vorontsov, V., Hallou, S., Fajardo, M., Kazamias, S., Lepape, S., Mercere, P., Morlens, A.S., Valentin, C. & Balcou, Ph. (2005). Progress in optical-field-ionization soft X-ray lasers at LOA. *Laser Part. Beams* **23**, 351–356.

Mulser, P., Cornolti, F. & Bauer, D. (1998). Modeling field ionization in an energy conserving form and resulting nonstandard fluid dynamics. *Phys. Plasmas* **5**, 4466–4475.

Murakami, M., Korobkin, O. & Horbatsch, M. (2013). High-harmonic generation from hydrogen atoms driven by two-color mutually orthogonal laser fields. *Phys. Rev. A* **88**, 063419.

Mur, V.D. & Popov, V.S. (1993). The Stark effect in strong fields: Perturbation theory, $1/n$-expansion and scaling. *Laser Physics* **3**, 462–474.

Ozaki, T., Elouga Bom, L.B., Ganeev, R., Kieffer, J.C., Suzuki, M. & Kuroda, H. (2007). Intense harmonic generation from silver ablation. *Laser Part. Beams* **25**, 321–325.

Reiss, H.R. (1980). Effect of an intense electromagnetic field on a weakly bound system. *Phys. Rev. A* **22**, 1786–1813.

Schafer, K.J., Yang, B., DiMauro, L.F. & Kulanderc, K.C. (1993). Above threshold ionization beyond the high harmonic cutoff'. *Phys. Rev. Lett*. **70**, 1599–1602.

Seres, J., Seres, E., Verhoef, A.J., Tempea, G., Streli, C., Wobrauschek, P., Yakovlev, V., Scrinzi, A., Spielmann, C. & Krausz, F. (2005). Laser technology: Source of coherent kiloelectronvolt X-rays. *Nature* **433**, 596–601.

Shiner, A.D., Trallero-Herrero, C., Kajumba, N., Bandulet, H.-C., Comtois, D., Legare, F., Giguere, M., Kieffer, J.-C., Corkum, P.B. & Villeneuve, D.M. (2009). Wavelength scaling of high harmonic generation efficiency. *Phy. Rev. L* **103**, 073902.

Shoucri, M. & Afeyan, B. (2010). Studies of the interaction of an intense laser beam normally incident on an overdense plasma. *Laser Part. Beams* **28**, 129–147.

Shuai, B., Shen, B., Li, R. & Xu, Z. (2002). High-order harmonic generation in ultra thin plasma foil. *Physica Scripta* **65**, 438–443.

Strelkov, V.V. (2006). Theory of high-order harmonic generation and attosecond pulse emission by a low-frequency elliptically polarized laser field. *Phys. Rev. A* **74**, 013405.

Svelto, O. (1998). *Principles of Lasers*. New York: Springer.

Tripathi, D., Bhasin, L., Uma, R. & Tripathi, V.K. (2010). Nonstationary ponderomotive self-focusing of a Gaussian laser pulse in a plasma. *Phy. Plasmas* **17**, 113113.

Yazdanpanah, J. & Anvary, A. (2012). Time and space extended particle in cell model for electromagnetic particle algorithms. *Phys. Plasmas* **19**, 033110.

Wang, W.M., Li, Y.T., Sheng, Z.M., Lu, X. & Zhang, J. (2013). Terahertz radiation by two-color lasers due to the field ionization of gases. *Phys. Rev. E* **87**, 033108.

https://doi.org/10.1017/S0263034616000112 Published online by Cambridge University Press